

The Tidal and Longer-period Circulation of Capricornia, Southern Great Barrier Reef

David A. Griffin,^A Jason H. Middleton^A and Lance Bode^B

^A School of Mathematics, University of New South Wales, P.O. Box 1, Kensington, N.S.W. 2033.

^B Department of Civil and Systems Engineering, James Cook University of North Queensland, Townsville, Qld 4811.

Abstract

Between June and December 1983, nine current meters and three water level recorders were deployed on the continental shelf and slope of the Capricornia Section of the Great Barrier Reef between Fraser Island (25°S.) and the mouth of the Capricorn Channel (23°S.) on the east coast of Australia. Tidal analyses of the hourly data set reveal an amplification of the semi-diurnal tides as they propagate north-westward into the Capricorn Channel. The results of a numerical model of tidal flow show excellent agreement with observations. The daily averaged (non-tidal) currents are highly variable and produce complex circulation patterns, but with a mean flow generally alongshore to the north-west. Comparisons with previous drifter studies and satellite-tracked buoy data suggest that the south-eastward flowing East Australian Current drives a large clockwise eddy, in the lee of the Swain Reefs, located east of the study region. It is postulated that this eddy, in addition to the generally north-westward wind stress, contributes to the north-westward flow within the study region. Temperatures recorded by the deployed instruments and temperature profiles from conductivity-temperature-depth casts confirm that tidal and longer period variability contribute to upwelling onto the continental shelf.

Introduction

The Capricornia section of the Great Barrier Reef (GBR) was the first part of the GBR to be proclaimed as a Marine Park. An understanding of the general circulation of the region is obviously of importance to management plans. However, little has been known of the dynamical oceanography of the region since the only previous observations of currents appear to be those from Woodhead's (1970) drifter study. More recently, Bode *et al.* (1981) have constructed a numerical model to investigate the tidal and wind-driven circulation, but this model needs verification from data.

The present study was designed to gain an understanding of the general circulation on the continental shelf between Fraser Island (25°S.) and the Capricorn Channel (23°S.). In this region the shelf has a width of ≈ 70 km, widening suddenly to over 200 km at the Capricorn Channel while the deep ocean rises from a depth of over 3000 m at 25°S. northward to the Capricorn Channel (Fig. 1). Since the transport processes affecting marine organisms have major contributions from both tidal and longer periods as a result of synoptic-scale meteorological forcing, a measurement program lasting 6 months was planned.

The dominant feature of the tides of the southern GBR was first reported by Flinders (1814) who noticed the exceptionally large and late tides in the vicinity of Broad Sound (22°S.). Middleton *et al.* (1984, hereafter MBH84) conducted theoretical and observational studies of the tides in and around Broad Sound and noted that the tide floods (ebbs) directly toward (away) from the Sound. The Broad Sound region is immediately to the north of the present study region and hence some influence is expected.

To the immediate north of the Capricorn Channel there have also been observational and theoretical studies of continental shelf waves (Middleton 1983; Middleton and Cunningham 1984). These were shown to be locally wind-driven but the dense reef on the outer section of this wide shelf modifies the wave propagation.

The present study is thus complementary to earlier studies to the north, both for tidal and longer periods. Griffin and Middleton (1986, hereafter GM86) have interpreted the longer-period variability observed in the present data set in terms of locally wind-driven barotropic and freely propagating baroclinic coastal trapped wave modes but little presentation of data was made. The present paper is concerned with a more detailed description of the observed physical features with less emphasis on interpretation.

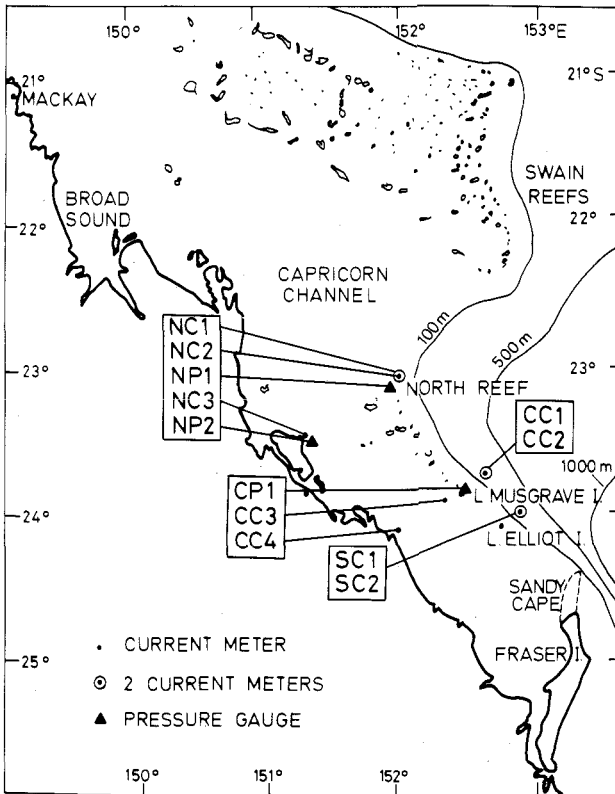


Fig. 1. Locations of deployed instruments within the study area.

The Field Program

In June 1983, six current-meter moorings and four pressure gauges ('water level recorders') were deployed in the study region from the CSIRO's RV *Sprightly*. Six months later they were retrieved using the charter boat *Sea Mare*. Three current-meter moorings, equipped with two current meters each, were deployed near the shelf break and the remaining three moorings were placed on the shelf proper with one current meter per mooring. Pressure gauges were deployed using SCUBA in less than 10 m of water on the outer edges of reefs. The locations of the three successfully retrieved pressure gauges and of the six current meter moorings are depicted in Fig. 1 which also shows the relationship of the study region to Broad Sound which is believed to be linked closely with the tides of the region. The instruments used were Aanderaa RCM4s and WLR5s, these being set to sample once an hour. All current meters were deployed far enough away from reefs so that local topography did not bias the measurements and deep enough so that swell-induced rotor overspeeding (Griffin 1987) was not a problem. Mooring details are listed in Table 1, the nomenclature of GM86 being retained.

Table 1. Instrument details and codes

The first letter N, C or S stands for northern, central and southern. The second letter C or P stands for current meter or pressure gauges. Numbering on each line starts at the deepest, most seaward instrument. The water depth listed for pressure gauges is the mean depth surrounding the reef on which the gauges were deployed

| Instrument line | Bottom depth (m) | Meter depth (m) | | Radial range and bearing (naut. miles) | (°T) | Record length (h) | Code |
|---|------------------|-----------------|----------------|--|------|-------------------|------|
| Northern (north Reef to Cape Capricorn) | 62 | 55 | N. Reef | 3.6 | 240 | 4084 | NC1 |
| | 62 | 45 | N. Reef | 3.6 | 240 | 4084 | NC2 |
| | 55 | 5 | N. Reef | n.a. | 140 | 4085 | NP1 |
| | 32 | 25 | C. Capricorn | 2.9 | 288 | 3915 | NC3 |
| | 14 | 2 | Rundle I. | n.a. | 140 | 3915 | NP2 |
| Central (Lady Musgrave I. to Round Hill Head) | 160 | 130 | L. Musgrave I. | 9.3 | 228 | 3666 | CC1 |
| | 160 | 70 | L. Musgrave I. | 9.3 | 228 | 4040 | CC2 |
| | 50 | 9 | L. Musgrave I. | 1.5 | 035 | 4034 | CP1 |
| | 40 | 33 | L. Musgrave I. | 4.8 | 077 | 1964 | CC3 |
| | 30 | 23 | Round Hill Hd. | 5.0 | 238 | 2969 | CC4 |
| Southern (Lady Elliot I.) | 160 | 130 | L. Elliot I. | 5.0 | 200 | 4052 | SC1 |
| | 160 | 70 | L. Elliot I. | 5.0 | 200 | 4052 | SC2 |

Table 2. Results of the tidal current analysis

A and B are the magnitudes (cm s^{-1}) of the semi-major and semi-minor axes of the current ellipses, while θ is the orientation (°T) of the semi-major axis in the flood tide direction. The letters *a* and *c* denote anticlockwise or clockwise current vector rotation. The Greenwich phase lag *g* is for GMT-10 and *F* is the form ratio $(O_1 + K_1)/(M_2 + S_2)$

| Component | | SC1 | SC2 | CC1 | CC2 | CC3 | CC4 | NC1 | NC2 | NC3 |
|-----------|----------|------|------|------|------|------|------|------|------|------|
| O_1 | A | 5.6 | 5.3 | 2.5 | 4.7 | 3.3 | 3.1 | 5.5 | 6.4 | 3.9 |
| | B | c0.6 | a1.5 | a0.9 | a2.1 | a1.6 | 0.0 | a1.9 | a2.1 | c0.8 |
| | θ | 313 | 275 | 281 | 291 | 290 | 306 | 289 | 292 | 329 |
| | <i>g</i> | 14 | 349 | 78 | 6 | 350 | 347 | 22 | 25 | 26 |
| K_1 | A | 5.4 | 8.9 | 3.2 | 7.5 | 5.2 | 4.5 | 9.0 | 10.8 | 7.8 |
| | B | c0.1 | a4.9 | a1.6 | a3.4 | a2.4 | c0.3 | a2.2 | a2.2 | c0.8 |
| | θ | 301 | 279 | 358 | 301 | 286 | 298 | 295 | 295 | 332 |
| | <i>g</i> | 58 | 23 | 43 | 67 | 64 | 25 | 68 | 60 | 63 |
| N_2 | A | 1.1 | 3.8 | 2.9 | 3.6 | 4.2 | 3.9 | 10.4 | 10.1 | 9.3 |
| | B | c0.5 | a0.8 | c1.0 | a1.3 | a0.4 | a0.3 | a0.8 | a0.4 | c1.2 |
| | θ | 284 | 270 | 250 | 269 | 261 | 286 | 286 | 285 | 327 |
| | <i>g</i> | 98 | 150 | 129 | 153 | 165 | 140 | 168 | 170 | 178 |
| M_2 | A | 6.3 | 13.1 | 8.0 | 15.7 | 14.0 | 16.2 | 36.8 | 44.3 | 38.5 |
| | B | c4.1 | a0.1 | c3.8 | a4.9 | a2.5 | c0.3 | a2.3 | a4.3 | c6.6 |
| | θ | 302 | 251 | 258 | 274 | 265 | 285 | 284 | 285 | 323 |
| | <i>g</i> | 146 | 168 | 138 | 179 | 165 | 164 | 183 | 187 | 199 |
| S_2 | A | 2.6 | 5.4 | 4.5 | 5.9 | 5.7 | 6.7 | 13.2 | 16.6 | 13.8 |
| | B | c1.0 | a1.5 | c0.5 | a2.4 | a1.0 | a0.3 | a1.5 | a1.9 | c2.0 |
| | θ | 294 | 255 | 258 | 279 | 264 | 292 | 286 | 284 | 324 |
| | <i>g</i> | 148 | 167 | 153 | 176 | 193 | 162 | 193 | 185 | 195 |
| <i>F</i> | | 1.23 | 0.77 | 0.46 | 0.56 | 0.43 | 0.33 | 0.29 | 0.28 | 0.22 |

Tides

Observed Tidal Currents and Weights

Tidal analyses were performed on all current vector and sea level data sets using the package developed by the Institute of Ocean Sciences, Patricia Bay, B.C., Canada (Foreman 1977, 1978). The method used is that of Godin (1972), being a least-squares fit to 69 tidal components.

Table 3. Results of the tidal height analysis
 H is the amplitude (cm) of the tidal height, g is for GMT-10 and F is the form ratio

| Component | | CP1 | NP1 | NP2 |
|-----------|-----|------|------|-------|
| O_1 | H | 11.8 | 13.9 | 14.7 |
| | g | 114 | 118 | 115 |
| K_1 | H | 21.6 | 25.8 | 26.7 |
| | g | 155 | 159 | 158 |
| N_2 | H | 15.1 | 19.6 | 25.4 |
| | g | 226 | 241 | 243 |
| M_2 | H | 65.4 | 84.1 | 110.3 |
| | g | 241 | 256 | 258 |
| S_2 | H | 23.5 | 31.8 | 42.0 |
| | g | 250 | 263 | 265 |
| F | | 0.38 | 0.34 | 0.27 |

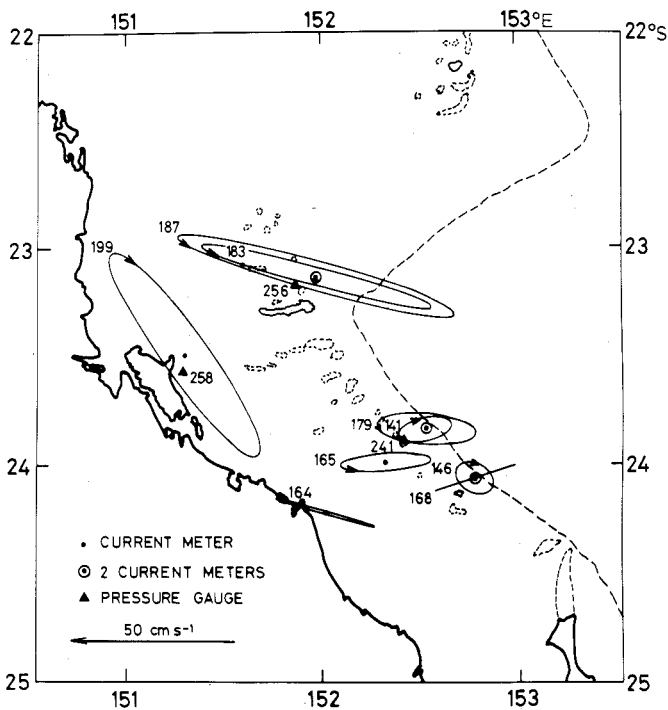


Fig. 2. Observed M_2 tidal current ellipses. Each ellipse is labelled with the Greenwich phase lag g of the flood tide and the sense of rotation is indicated. At dual meter moorings, the deeper currents are distinguished by their smaller amplitudes. Pressure gauges are labelled with their high tide g values.

The results for the five major constituents are listed in Table 2 (currents) and Table 3 (heights). The Greenwich phase lag g is listed rather than the Greenwich Epoch G because the former is usually favoured due to its computational convenience. The two are related by $g(j) = G - j\sigma|360|$, where j is the time zone (in hours, negative for LMT ahead of GMT) and σ is the frequency of the component in degrees per hour. The form ratio $F = (O_1 + K_1)/(M_2 + S_2)$ is also listed and provides a measure of the relative importance of the diurnal and semidiurnal components.

The pattern revealed is as anticipated in the light of Flinders' (1814) observations and the theory and observations of MBH84. The flood tide directions, rather than being simply onshore, have a strong alongshore component towards Broad Sound. The flood tide phases and amplitudes indicate later and stronger tidal currents closer to Broad Sound.

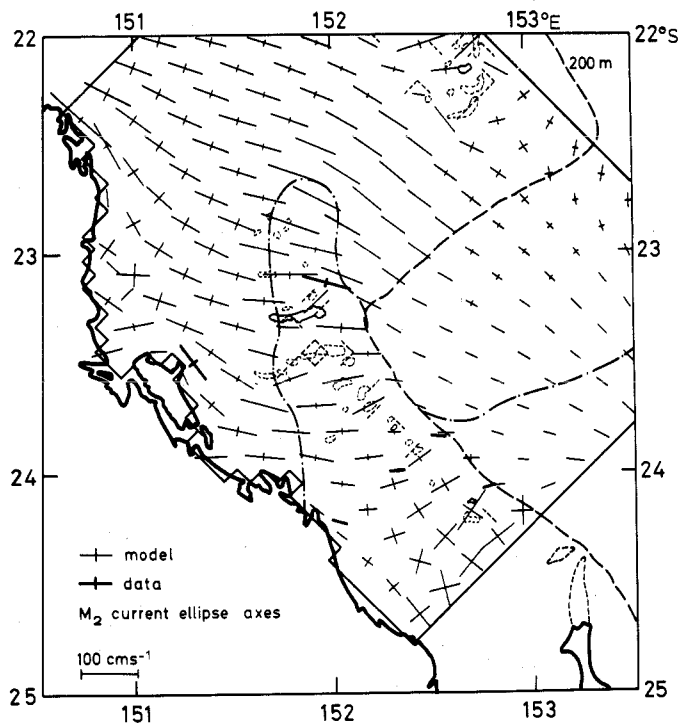


Fig. 3. Comparison of the numerical model's predicted M_2 current ellipse axis lengths and orientations with those observed. Data from the top meter only is shown for dual meter moorings. Only every second grid point (in each direction) of the model is plotted and the zero minor axis contour is shown as a dot-dash line. A solid boundary is drawn around the computational region of the model and resolvable reefs are drawn dashed.

These features are demonstrated in Fig. 2 which shows the M_2 current ellipses and phases. Other components show a similar behaviour. The tidal heights and their phases as shown in Fig. 2 also show larger and later tides closest to Broad Sound.

Whilst the general picture is the same for all components, the degree of amplification as Broad Sound is approached is greatest for the semidiurnal components. The form ratio F has a minimum of 0.22 at NC3, the coastal meter closest to Broad Sound where the tides may be classified as semidiurnal ($F < 0.25$). Farther from Broad Sound or closer to the open ocean the value of F increases so that the tides are classified as mixed, semidiurnal ($0.25 < F < 1.50$). The highest value of F within the study region is for SC1, the deep meter farthest from Broad Sound, where the diurnal and semidiurnal constituents are nearly equal.

Comparing the phase lags listed in Tables 2 and 3 for neighbouring current meters and pressure gauges reveals that the high tide lags the flood tide by 90° – 110° for the diurnal and 60° – 80° for the semidiurnal components. This shows that the tide most resembles a standing wave (lag = 90°), but with a smaller progressive component to the south-east (lag = 180°) for the diurnals and to the north-west (lag = 0°) for the semidiurnals.

The senses of rotation of the current vectors reveal a pattern which is not presently understood. The predominant sense of rotation of near-surface currents is anticlockwise while the two meters at 130 m depth recorded clockwise rotation. Exceptions to these rules (disregarding near-rectilinear currents) include all components at NC3 and the diurnal components at CC1. MBH84 report anticlockwise rotation north of Mackay and clockwise rotation to the south. The observed prevalence of anticlockwise rotation within the present study region is the only feature of the tides at apparent odds with the findings of MBH84.

The M_2 Tide

In this subsection the observed M_2 tide is compared with the predictions of a numerical model. The details of the model are discussed by Bode *et al.* (1981). Briefly, it is a barotropic model on an f -plane with non-linear horizontal advective terms included. The appropriate momentum equations are solved by explicit finite differences on a Richardson lattice. Reefs large enough to be resolved by the grid (spacing 5 nautical miles) are modelled as shallow weirs. The model is driven by the limited offshore tidal data that existed prior to the present study.

The observed current ellipses are compared in Fig. 3 with those predicted by the model. The overall agreement is excellent despite the topographic complexity of the region, there being no significant discrepancies between the observed and modelled ellipse axis orientations or magnitudes. The model's zero minor axis contour, which delineates regions of oppositely rotating current vectors, is also shown in Fig. 3. All but one of our meters were in the region of predicted anticlockwise rotation and the observations are in accord with the model on this point.

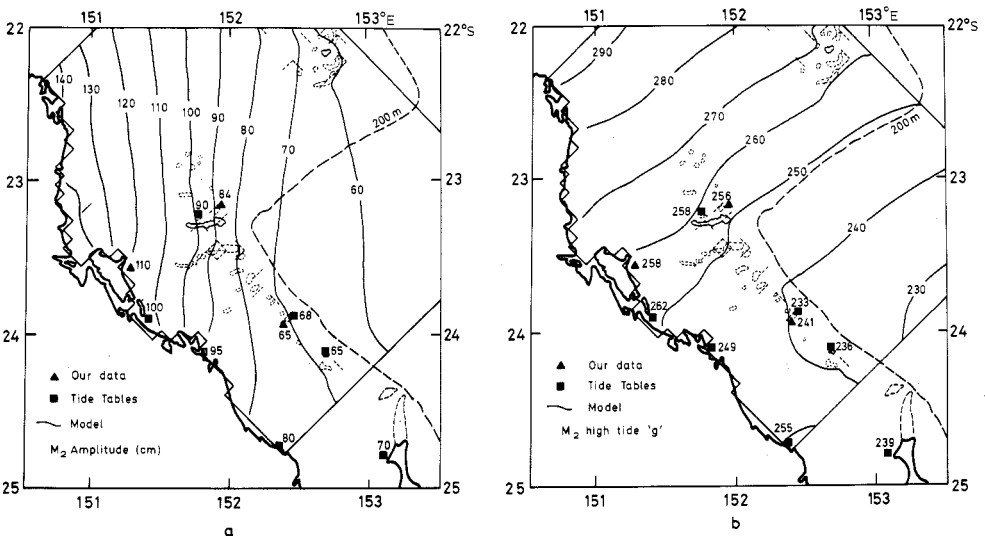


Fig. 4. Comparison of the numerical model's predicted M_2 tidal height (a) and Greenwich phase lag (b) fields with our own and previous observations.

The model is perhaps more fairly judged by its predictions of tidal heights and their phases since these are less affected by local topography. Fig. 4a shows tidal height amplitudes and Fig. 4b Greenwich phases of high tide as predicted by the model for comparison with

observation. The agreement with previously tabulated data is good but, encouragingly, even better with our observations.

The effect of the reefs on the tide is perhaps the most challenging aspect of modelling the Great Barrier Reef (Bode *et al.* 1981). The model predicts some phase retardation by the reefs and a slight reduction of tidal heights. Figs 4a and 4b depict an upper limit of the estimated effect of the reefs. While the present data set cannot test these predictions in particular, it does nevertheless show that the salient features of the M_2 tide within the study region are well predicted by the model.

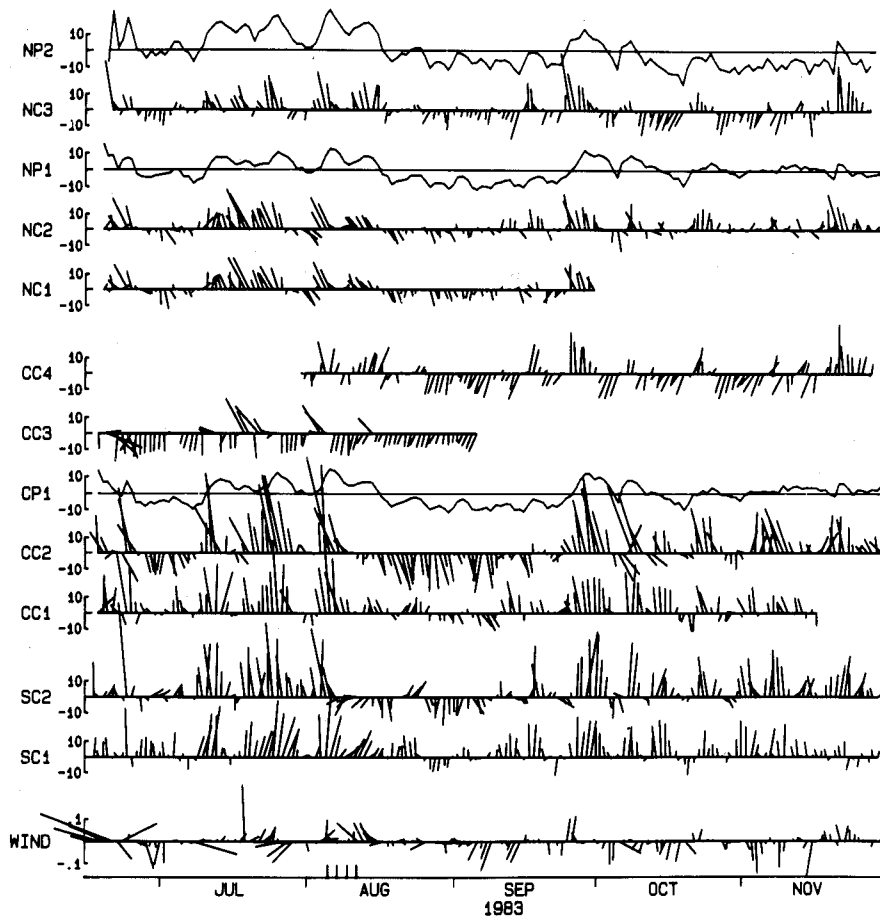


Fig. 5. The data set (tides removed) from instruments within the study region. The original hourly data set has been filtered to remove energy at periods less than 40 h then subsampled at daily intervals. Current vectors pointing straight up the page are directed locally alongshore. Velocity is in centimetres per second. Total pressure is expressed in centimetres of seawater. Wind stress is an average of two offshore stations and is plotted in Newtons per square metre. Grid marks on the time axis concern Figs 6a-6d.

Longer-period Circulation

To examine the circulation due to currents having periods substantially longer than the (diurnal) tidal and inertial (29.4 h) periods, the hourly data set was filtered with a Fourier transform filter to remove energy at periods less than 40 h and then subsampled at daily intervals. The resulting daily data set of sea level, currents and wind stress (Sandy Cape and Lady Elliot I. averaged) is presented in Fig. 5. The 'sea level' traces are actually total pressure

(sea pressure plus atmospheric) expressed in centimeters of seawater. [Some authors appear to have neglected the fact that Aanderaa WLR5 (or similar) units record pressure, not sea level, and hence do not see the 'inverse barometer effect' as they do with float-operated devices.]

The flow is obviously dominated by periodic (period 6–10 days) north-westward pulses of current. Current speeds in excess of 30 cm s^{-1} were recorded off the shelf break and these often persisted for several days. Between these events, return flow to the south-east was generally much weaker, resulting in net north-westward flow, the reason for this being unclear. On the shelf proper, currents had smaller amplitudes and were more evenly distributed about zero. Sea level (pressure) fluctuations were generally in geostrophic equilibrium with the alongshore current. In GM86 it was shown that the 6–10-day period motions may be expressed as a sum of baroclinic coastal trapped wave modes whose energy source is south of Fraser I. The higher modes were shown to be important in accounting for (i) the relatively high amplitude currents seen off the shelf break, (ii) the fact that these pulses of current occur a day later off Lady Musgrave I. than off Lady Elliot I., and (iii) the amplitude of the temperature fluctuations recorded off the shelf break (see next section). It was shown that the local wind stress is not a significant contributor to the strong currents observed over the continental slope but that most of the energy had propagated from farther south along the continental slope. Local wind stress only contributed significantly to the currents over the shelf proper.

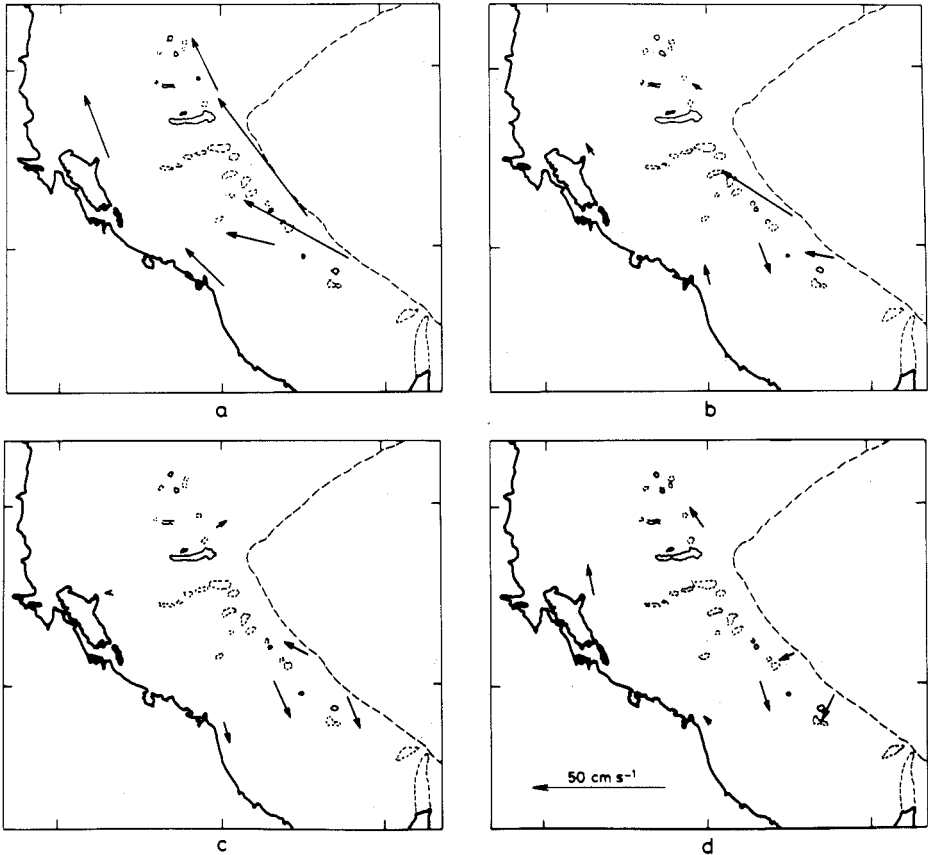


Fig. 6. (a)–(d) Observed (tides removed) current fields for the 4 days indicated on the time axis of Fig. 5. The nearer surface current only is shown for dual meter moorings.

The resulting circulation within the study region is highly complex. While the circulation due to each coastal trapped wave mode is comparatively simple (GM86, fig. 13), the combination of several modes propagating at different speeds produces a complex circulation that changes quite rapidly with time. This is demonstrated in Fig. 6 which shows a sequence of recorded current vectors in their geographic context. The interval between frames is 2 days, with Fig. 6a representing 5 August 1983, a day of strong north-westward flow throughout the region. The circulation depicted by Figs 6b, 6c and 6d, representing 2, 4 and 6 days later, is clearly quite complicated, in obvious defiance of any simple model. This level of complexity may be assumed to be typical of the region.

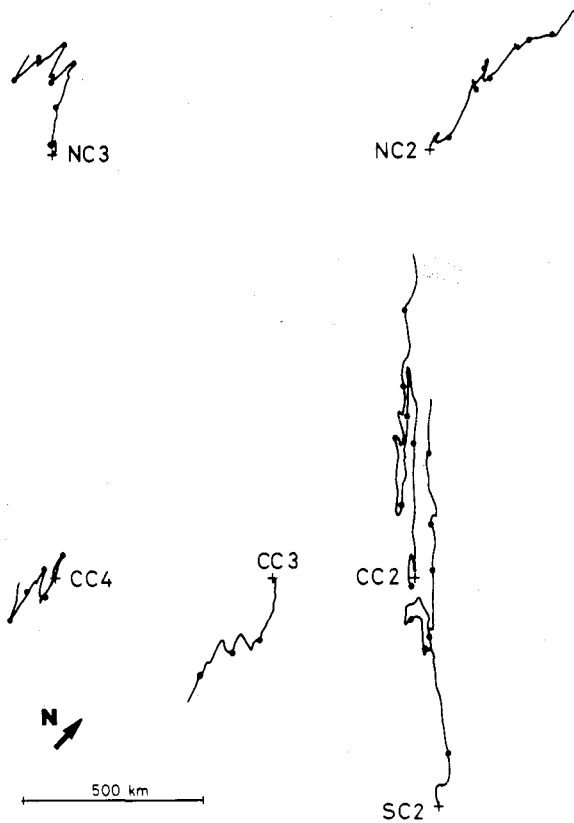


Fig. 7. Progressive vector diagrams of currents (nearer surface at dual meter moorings) arranged to represent their relative geographic positions. The scale refers only to the particle virtual displacements, not the separation of the instruments. Dots are drawn at intervals of 20 days.

Whilst the 6–10-day period oscillatory components of the current are complex, the mean flow within the region is much simpler, as can be seen from Fig. 7 which shows progressive vector diagrams of the currents within the study region. The origin of each particle 'track' is indicative of the relative placing of the instrument concerned, but the distance scale refers only to particle 'displacements'. Since the particle 'displacements' greatly exceed the separation of instruments and the flow has been shown to be complex, Fig. 7 must be interpreted with caution. However, it is clear that the mean flow is predominantly parallel to isobaths, being north to north-westward everywhere except at CC3 and CC4 which recorded southward and little net flow, respectively.

These findings, however, are difficult to reconcile with the conclusions of Woodhead (1970). Direct comparisons with that study are not possible because our meters were moored at least 23 m below the surface while Woodhead's drifters were drogued at only 1 m depth. Also, interannual variations cannot be discounted. Nevertheless, the following comments on Woodhead's study can be made.

Within 3 months of release, about 19% of Woodhead's drifters had become stranded. Woodhead observed that there was more dispersion of the drifters than anticipated but that most drifters released near our study region became stranded on the nearby coastline. Woodhead hence deduced a mean southward, or cross-isobath, flow. Woodhead's figs 4-7 show the drifter release and stranding points. If the drifter paths are drawn as straight lines, distances of 20-100 km (for drifters released over the shelf) are involved, with many paths crossing each other at near right angles. From the present study it is known that in 3 months typical shelf proper currents make drifter tracks of several hundred kilometers quite possible. Hence, it is likely that the drifters travelled considerable distances back and forth along the shelf, effectively randomizing their release point identities before being gradually blown ashore by the predominantly south-easterly winds. Pickard *et al.* (1977) discussed the possibility that Woodhead incorrectly discounted the effect of wind-forcing.

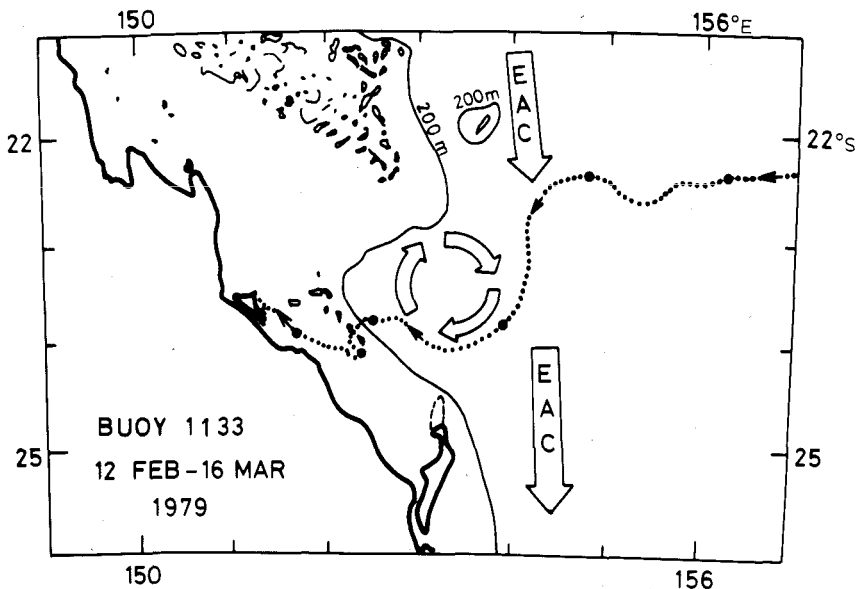


Fig. 8. The track of a satellite tracked buoy showing the influence of the East Australian Current and a postulated lee eddy. Dots are drawn at intervals of 5 days.

A considerable number of drifters became stranded south of Fraser I. but the present study has shown that the predominant current off Lady Elliot I. is north-westward. Unless these seemingly contradictory results are due to interannual differences, the most likely explanation is that the south-eastward flowing East Australian Current (EAC) generates a large lee eddy south of the Swain Reefs, resulting in north-westward backflow near the Capricornia shelfbreak. Hence, it would be likely that drifters dropped into the eddy at any location could eventually join the main flow of the EAC and head south. Many of Woodhead's other 'anomalous' strandings are explained if the drifters are allowed to complete or nearly complete orbits within this eddy.

The postulated position of such an eddy is shown in Fig. 8 which also shows the path taken by a satellite-tracked buoy (Greig 1980) which drifted into the area. Although the

position and width of the EAC at that time is unknown, the flow indicated is likely. The buoy track is certainly consistent with the hypothetical eddy and with the flow field within the study region suggested by the present observations. However, such an eddy may not necessarily be a permanent feature of the region. As can be seen from Fig. 5, there is a long (≈ 90 day) period variation of the average current which could be due to the appearance and disappearance of this eddy as the East Australian Current fluctuates. The north-westward mean wind stress doubtlessly also contributes to the north-westward mean flow but it is of insufficient strength to account for the strong currents observed off Lady Elliot and Lady Musgrave Islands.

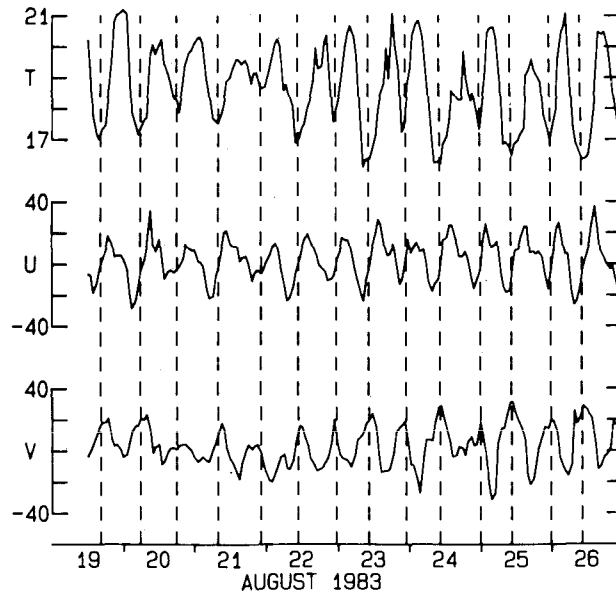


Fig. 9. A sample period of hourly temperature (T , $^{\circ}\text{C}$), across-shelf (U) and alongshelf (V) components (cm s^{-1}) of current. The data are from CCI, at 130 m depth off Lady Musgrave I., where 305°T is the local alongshelf direction.

Thermocline Motion

The current meters and pressure gauges were equipped with thermistors which recorded temperature hourly along with the current or pressure. Temperatures recorded by the current meters nearest to the coast exhibited no tidal or daily period variation. Nearer the shelf break, off North Reef, however, some tidal signal was observed. Temperature was reduced by up to 2°C by an incoming spring tide. The pressure gauges all recorded daily rather than tidal period temperature fluctuations of up to 4°C presumably because they were deployed in shallow water on reef edges and hence subject to solar heating. The current meters at 60 m depth in water 160 m deep recorded temperature variations but these were often due simply to mooring layover. The meters at 130 m depth, however, which were not subject to much layover recorded the most striking temperature fluctuations. These fluctuations are clearly tidally induced as can be seen from Fig. 9 which shows a sample period of 7 days of hourly current and temperature records. The clockwise rotation of the current vector (as listed in Table 2) is clearly evident. Temperature is $\approx 90^{\circ}$ behind the offshore component of current, i.e. temperature minima occur at the end of the incoming tide as is to be expected.

The onshore current amplitude (from Fig. 9) is $\approx 25 \text{ cm s}^{-1}$. At the semidiurnal frequency (assuming locally isotropic current amplitudes) the fluid particle onshore displacement

amplitude is hence about 3.5 km, at which distance offshore the water is approximately 60 m deeper. This means that the fluid particle vertical displacement amplitude is perhaps as large as 60 m, which would account for the large ($\approx 1.5^\circ\text{C}$) amplitude of the temperature variation, given the observed temperature decrease with depth (Fig. 11).

In addition to tidally induced thermocline motion, the instruments also recorded temperature fluctuations due to longer-period phenomena. Fig. 10 presents the low-pass filtered daily temperature data set from all recording instruments deployed within the study region. The seasonal variation of coastal water temperature is easily seen but of perhaps greater interest are the (fairly irregular) 6–10-day period temperature fluctuations recorded by the central and southern instruments near the shelf break and over the continental slope. The amplitudes of the fluctuations are comparable with the tidal frequency amplitudes and were shown in GM86 to be related to the alongshore current associated with the passage of second or third mode coastal trapped waves. These waves resemble internal baroclinic Kelvin waves over the continental slope, with thermocline motion trapped against the slope, propagating along it at only $\approx 0.5 \text{ ms}^{-1}$.

Hence there appear to be two mechanisms operating independently on different time scales to bring colder, presumably nutrient-rich, water from greater depth over the continental slope up and onto the continental shelf. The combined effect of the two mechanisms is of course additive.

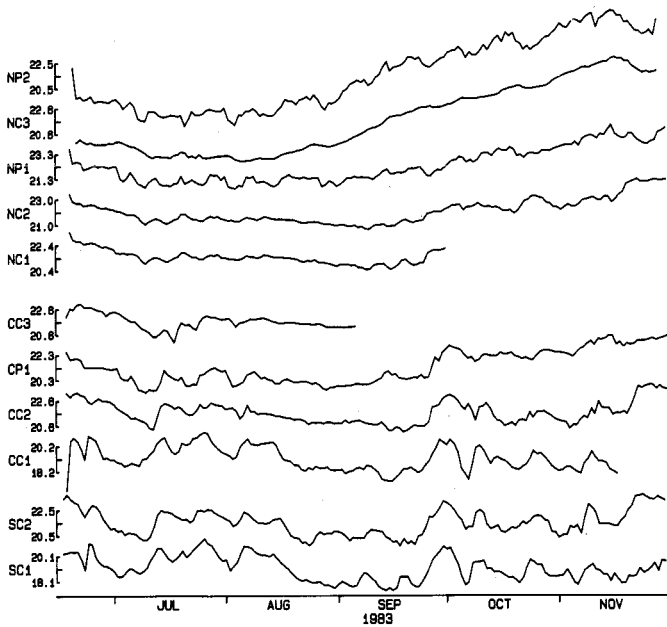


Fig. 10. Temperature ($^\circ\text{C}$)-time series (filtered) from all recording instruments.

Limited conductivity-temperature-depth (CTD) surveys were carried out on the deployment (June) and retrieval (December) cruises. Data from the central mooring line deployment transect are shown in Fig. 11. Two casts from mid-shelf clearly show the presence, at depths of 25–35 m, of water which shares the temperature and salinity properties of water from depths of 90–100 m over the continental slope, supporting the hypothesis that the above mechanisms are effective.

Hatcher and Larkum (1983) showed that nitrogen concentration is the limiting factor for biomass production on One Tree Reef, within the present study region. Hence, it is now suggested that the two upwelling mechanisms (tidal pumping and coastal trapped waves) discussed above could be very important to the sustainment of the reef ecosystems within the study region.

The intermittency of this upwelling is possibly demonstrated by the fact that the December CTD survey (not shown) revealed no pool of dense water over the shelf, the only stratification being a very shallow thermocline. An intrusion of cold water was, however, detected near the shelf break off North Reef.

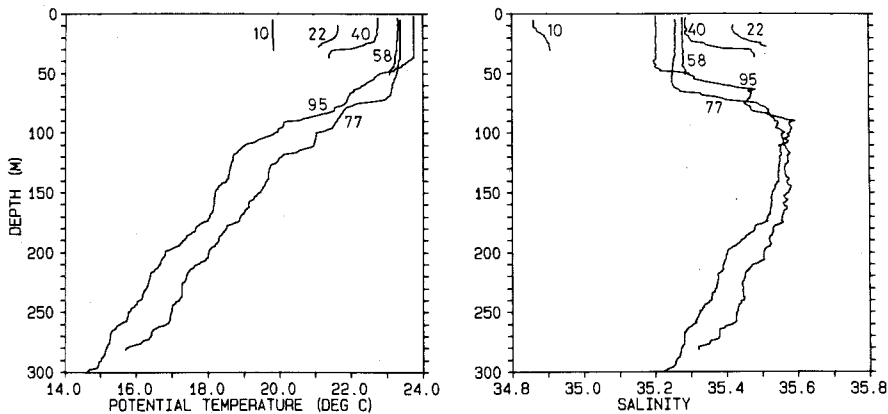


Fig. 11. Temperature and salinity profiles from a CTD transect along the central line of meters performed on the deployment cruise. Traces are labelled with the distance (km) from the coast. The three most seaward casts were outside the coral reefs along the shelf break.

Conclusions

This study has shown that the tidal heights and currents over the shelf proper within Capricornia are well predicted by the barotropic numerical model of Bode *et al.* (1981). However, such modelling techniques are incapable of incorporating the observed tidally induced upwelling. Three-dimensional stratified modelling would be required to investigate this phenomenon. Such work would be motivated by the possible importance of tidal pumping to the reef ecosystems. This mechanism has been reported to be significant at other locations on the GBR by Thompson and Golding (1981), Thomson and Wolanski (1984) and Airey (personal communication).

Non-tidal currents within the study region are highly variable, although a north-westward mean flow is a fairly persistent feature. Three forcing mechanisms seem to operate: the local wind stress, coastal trapped waves propagating from south of Fraser Island and the postulated backflow of an East Australian current lee eddy south of the Swain Reefs. The wind has been shown to have less importance locally than expected in the light of other observations from the GBR (Middleton and Cunningham 1984) so that the latter two forcing mechanisms appear to be dominant. These, however, are less well understood than direct wind forcing and require further investigation. Associated with the coastal trapped waves is a significant thermocline motion which appears to be responsible (in addition to the tides) for periodic up- and down-welling. This lower frequency motion has been shown by Andrews and Gentien (1982) to contribute to the GBR nutrient requirements farther north of the present region.

Acknowledgments

This work was supported by Australian Marine Sciences and Technologies Grants Scheme grants 82/1137 and 81/117. David Griffin is grateful to the Commonwealth Postgraduate Research Awards scheme for support during his Ph.D. candidature. We would like to thank Greg Nippard for his field work and electronics expertise, Luciano Mason for expert assistance with the numerical modelling, the CSIRO for time on RV *Sprightly*, Jenny

Pragnell (CSIRO) for CTD data preparation, George Cresswell and Graham Wells (CSIRO) for the buoy track data, Cathy Faust for drafting the figures and Rhona Metzker for typing the manuscript.

References

- Andrews, J. C., and Gentien, P. (1982). Upwelling as a source of nutrients for the Great Barrier Reef ecosystems: a solution to Darwin's question? *Mar. Ecol. Prog. Ser.* **8**, 257-69.
- Bode, L., Mason, L. B., Sobey, R. J., and Stark, K. P. (1981). Hydrodynamic studies of water movements within the Great Barrier Reef region. I. Preliminary investigations. Research Bulletin (James Cook University of North Queensland Department of Civil and Systems Engineering) No. CS27.
- Flinders, M. (1814). 'A Voyage to Terra Australis.' Vol. 2. (G. & W. Nicol: London.)
- Foreman, M. G. G. (1977). Manual for tidal heights analysis and prediction. Pacific Marine Science Report 77-10. (Institute of Ocean Sciences, Patricia Bay, Victoria, B.C.)
- Foreman, M. G. G. (1978). Manual for tidal currents analysis and prediction. Pacific Marine Science Report 78-6. (Institute of Ocean Sciences, Patricia Bay, Victoria, B.C.)
- Godin, G. G. (1972). 'The Analysis of Tides.' (University of Toronto Press.)
- Greig, M. A. (1980). Satellite-tracked buoy data report. V. Bureau of Meteorology buoys tracked in the southern Indian and Pacific Oceans January to March, 1979. CSIRO Aust. Division of Oceanography Rep. No. 120.
- Griffin, D. A., and Middleton, J. H. (1986). Coastal trapped waves behind a large continental shelf island, southern Great Barrier Reef. *J. Phys. Oceanogr.* **16**, 1651-64.
- Griffin, D. A. (1987). Mooring design to minimise Savonius rotor overspeeding. *Cont. Shelf Res.* (In press.)
- Hatcher, B. G., and Larkum, A. W. D. (1983). An experimental analysis of factors controlling the standing crop of the epilithic algal community on a coral reef. *J. Exp. Mar. Biol. Ecol.* **69**, 61-84.
- Middleton, J. H. (1983). Low frequency trapped waves on a wide reef-fringed continental shelf. *J. Phys. Oceanogr.* **13**, 1371-82.
- Middleton, J. H., Buchwald, V. T., and Huthnance, J. M. (1984). The anomalous tides near Broad Sound. *Cont. Shelf Res.* **3**, 359-81.
- Middleton, J. H., and Cunningham, A. (1984). Windforced continental shelf waves from a geographical origin. *Cont. Shelf Res.* **3**, 215-32.
- Pickard, G. L., Donguy, J. R., Henin, C., and Rougerie, F. (1977). A review of the physical oceanography of the Great Barrier Reef and Western Coral Sea. Australian Institute of Marine Science Monograph Series. Vol. 2.
- Thompson, R. O. R. Y., and Golding, T. J. (1981). Tidally induced 'upwelling' by the Great Barrier Reef. *J. Geophys. Res.* **86**, 6517-21.
- Thomson, R. E., and Wolanski, E. J. (1984). Tidal period upwelling within Raine Island entrance Great Barrier Reef. *J. Mar. Res.* **42**, 787-808.
- Woodhead, P. M. J. (1970). Sea surface circulation in the southern region of the Great Barrier Reef, Spring 1966. *Aust. J. Mar. Freshw. Res.* **21**, 89-102.